

QCD coherence in deep inelastic scattering at small x at HERA

K. Golec-Biernat¹

Department of Physics, University of Durham, Durham DH1 3LE, England

L. Goerlich² and J. Turnau³

Institute of Nuclear Physics, ul. Kawiory 26a, 30-055 Kraków, Poland

Abstract

QCD coherence effects in initial state radiation at small x in deep inelastic scattering in HERA kinematics are studied with the help of the Monte Carlo model SMALLX. Theoretical assumptions based on the CCFM evolution equation are reviewed and the basic properties of the partonic final states are investigated. The results are compared with those obtained in the conventional DGLAP evolution scheme.

¹On leave from Institute of Nuclear Physics, Kraków, Poland; e-mail: K.J.Golec@durham.ac.uk

²e-mail:goerlich@chall.ifj.edu.pl

³e-mail:turnau@chall.ifj.edu.pl

1 Introduction

HERA is the first accelerator which allows one to study experimentally the region of low values of the Bjorken variable x in deep inelastic lepton-proton scattering ($x \sim 10^{-5}$ and $Q^2 > 1 \text{ GeV}^2$). It is, therefore, particularly important to analyze experimental results in this kinematical region with the help of theoretical models which contain essential features of QCD in the small- x limit.

Angular ordering (**coherence**) in initial state gluon radiation (ISR), imposed on real and virtual gluon emission at small x , is one of the most important features of perturbative QCD in the small- x limit [1, 2, 3]. The dominant contribution to ISR is given by multi-gluon amplitudes with angular ordering of subsequent gluon emissions. Outside the angular ordered regions of phase space destructive interference takes place and amplitudes cancel. This phenomenon can be formulated in a probabilistic framework as a branching process, in which the gluon structure function at small x is obtained after a summation of large $\log(1/x)$ powers corresponding to infrared and collinear singularities coming from the angular ordered regions of phase space. The resummation is effectively done with the help of the CCFM evolution equation [2, 3].

The $\log(1/x)$ terms resulting from angular ordering are subleading with respect to large logarithms obtained in the multi-Regge kinematics¹ leading to the BFKL evolution equation [4]. In a fully inclusive quantity like the gluon structure function the subleading logarithms cancel, and the CCFM and BFKL evolution equation are equivalent. This is not true, however, for exclusive processes for which the “*angular*” logarithms give important contribution to the final state structure [3]. Therefore, the branching process with angular ordering is indispensable for the final state description.

SMALLX is the Monte Carlo model [5, 6] which incorporates the CCFM branching scheme in the initial state gluon radiation. For an alternative Monte Carlo model which also uses the CCFM branching see [7]. The dominant process at small x – the quark-antiquark pair production accompanied by gluon radiation, see Fig.1, – is generated using two approximations for gluon emission. The first approximation, called **all-loop** and given by the CCFM branching scheme with angular ordering for all x values, is compared with a conventional branching, called **one-loop**, leading to the DGLAP evolution equations with angular ordering at large x and transverse momenta ordering for small- x values [8, 9]. The two branching schemes coincide at large x but differ significantly when x is small. The cross section for the discussed process is obtained using the k_{\perp} -factorization theorem [10], in which the off-shell boson-gluon fusion cross section is convoluted with the gluon structure function computed in the two branching schemes.

The aim of this paper is the analysis of angular ordering effects in DIS in the small- x HERA kinematics with the help of the SMALLX Monte Carlo program. The comparison between the CCFM (all-loop) and DGLAP (one-loop) branching schemes plays an important role in this analysis. The main idea is to fix the parameters of generation in both approximations separately such that a reasonable agreement with the measured inclusive cross section is obtained. We choose the charm structure function data from HERA for

¹In this kinematics emitted gluons are strongly ordered in rapidity and have comparable transverse momenta.

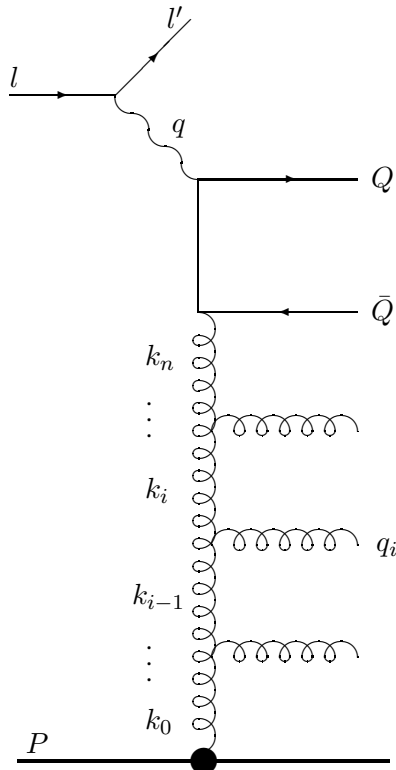


Figure 1: The process generated in SMALLX.

this purpose. Then, we study various exclusive final state characteristics to show the effect of angular ordering. This is done in accord with the present belief that only exclusive measurements can discriminate between mechanisms of QCD evolution.

The paper is organized as follows. In section 2 we briefly describe the process under consideration. This includes discussion of the process kinematics, gluon branching schemes and their relation to the CCFM and DGLAP evolution equations. In section 3 we describe the details of Monte Carlo generation pointing out the crucial elements discussed later in section 4 devoted to the results of our Monte Carlo studies.

2 Description of the process

2.1 Cross section and kinematics

The process generated in SMALLX, dominating electron-proton DIS at small value of the Bjorken variable x_B , is shown in Fig. 1. A quark-antiquark pair is produced accompanied by initial state gluon radiation.

In the high energy limit $\sqrt{s} \gg M$, where M is a quark mass, the cross section for this process is given by a convolution of the hard subprocess $\gamma g \rightarrow Q\bar{Q}$ cross section $\hat{\sigma}$, and the unintegrated gluon structure function \mathcal{F} describing gluonic emission [10]

$$\sigma = \frac{\alpha_{em}}{2\pi} \int \frac{dx}{x} \frac{dy}{y} \frac{dq^2}{q^2} d^2\mathbf{k}_\perp \{1 + (1-y)^2\} \mathcal{F}(x, \mathbf{k}_\perp, \mu) \hat{\sigma}(M; k, q), \quad (1)$$

where y is the standard DIS kinematical variable, $q \simeq yl + q_\perp$ and $k = k_n \simeq x_n P + k_\perp$ are the virtual photon and the last exchanged gluon momenta respectively (l and P are the incident lepton and proton momenta), and μ is a hard scale to be discussed later. It is important to stress that $\hat{\sigma}$ is the **off-shell** cross section, which means that the virtuality of the gluon, $k^2 = k_\perp^2 = -\mathbf{k}_\perp^2$, is different from zero. This allows a smooth limit of $\hat{\sigma}$ when a quark mass $M \rightarrow 0$ since the gluon virtuality k_\perp^2 regulates a potential divergence present in the **on-shell** version of this cross section, see [5, 6] for more details.

The whole information about the initial state gluon emission is contained in the un-integrated gluon distribution function $\mathcal{F}(x, \mathbf{k}_\perp, \mu)$ obeying the CCFM equation [2] which sums angular ordered gluonic emissions, for both large and small x_B . This equation allows a representation of \mathcal{F} in terms of branching processes, which is convenient for Monte Carlo simulation. Before discussing this representation it is necessary to describe kinematics of the gluonic emission.

The momenta of exchanged space-like gluons k_i , and final state real gluons $q_i = k_{i-1} - k_i$, are decomposed into a longitudinal and transverse components (Sudakov decomposition)

$$k_i = x_i p + \bar{x}_i \bar{p} + k_{\perp i} , \quad (2)$$

where the p and \bar{p} are null vectors ($2p \cdot \bar{p} = s$) and $k_{\perp i} \cdot p = k_{\perp i} \cdot \bar{p} = 0$. In the frame in which p and \bar{p} are collinear, $p \sim (1, 0, 0, 1)$ and $\bar{p} \sim (1, 0, 0, -1)$, we have $k_\perp = (0, \mathbf{k}_\perp, 0)$.

Each emission is characterized by the branching variable $z_i < 1$, being the fraction of the $k^+ (= k_0 + k_3)$ component of the exchanged momentum k_{i-1} lost due to emission of the gluon q_i

$$z_i = \frac{k_i^+}{k_{i-1}^+} = \frac{x_i}{x_{i-1}} . \quad (3)$$

Notice the obvious relation

$$x_n = z_n z_{n-1} \dots z_1 x_0 , \quad (4)$$

which implies that the small- x limit of the branching process is not necessary related to small values of the branching variables. In order to characterize the phase space of multi-gluon emission it is convenient to define the **rescaled** transverse momentum of emitted gluons

$$q'_{\perp i} \equiv \frac{q_{\perp i}}{1 - z_i} = x_{i-1} \sqrt{s} \tan\left(\frac{\theta_i}{2}\right) , \quad (5)$$

where from now $q_{\perp i} = |\mathbf{q}_{\perp i}|$ is the length of the transverse component and θ_i is the emission angle of the massless final state gluon, defined with respect to the z -axis of the collinear frame.

In the approximation leading to the CCFM equation (**all-loop** approximation) the dominant contribution to the multi-gluon emission process comes from a part of phase space with **angular ordering** of subsequent emissions

$$\theta_i > \theta_{i-1} \quad \Leftrightarrow \quad q'_{\perp i} > z_{i-1} q'_{\perp i-1} , \quad (6)$$

where the equivalence results from relations (5). We additionally introduce the **collinear cutoff** $q_0 \equiv z_0 q'_{\perp 0}$ for the first real gluon emission: $q'_{\perp 1} > q_0$. Outside of the angular

ordered region destructive interference takes place and multi-gluon emission amplitudes cancel. Notice that in the limit $z_i \ll 1$ condition (6) practically does not restrict the ordinary transverse momenta: $q_{\perp i} \approx q'_{\perp i} > 0$.

This is not the case in the conventional DGLAP (**one-loop**) approximation, in which a more restrictive condition is imposed

$$q'_{\perp i} > q'_{\perp i-1}, \quad (7)$$

and $q'_{\perp 1} > q_0$. Notice that since $q'_{\perp i-1} > z_{i-1} q'_{\perp i-1}$, condition (7) implies angular ordering for all values of z . For $z_i \approx 1$ conditions (7) and (6) are equivalent, but for $z \rightarrow 0$ the transverse momentum ordering $q_{\perp i} > q_{\perp i-1}$ is additionally imposed in the one-loop case on the angular ordered multi-gluon emission. Therefore, the one-loop phase space is much smaller than in the all-loop case.

2.2 Branching probabilities

Having the momentum k_{i-1} of the exchanged gluon, the k_i and q_i momenta can be constructed provided the branching variable (3) and the rescaled transverse momentum (5) are known. Therefore, a chain of subsequent gluon emissions is obtained in which the branching variables $(z_i, q'_{\perp i})$ are generated with the probability $d\Pi_i$, given in the all-loop approximation by

$$d\Pi_i = \Delta_S(i, i-1) P_g(i) \Theta(q'_{\perp i} - z_{i-1} q'_{\perp i-1}) \Theta(1 - z_i - Q_0/q'_{\perp i}) \frac{d^2 \mathbf{q}'_{\perp i}}{\pi \mathbf{q}'_{\perp i}{}^2} dz_i \quad (8)$$

where Δ_S and P_g are functions of branching variables in a shorthand notation to be discussed below. The first Θ step function imposes angular ordering condition (6) on generated real gluon momenta, whereas the second one allows only emissions with the transverse momentum $q_{\perp i} = (1 - z_i) q'_{\perp i} > Q_0$ to regularize soft singularity in the real gluon emission, manifest at $z_i = 1$ in the function P_g (eq.(10)).

The function Δ_S , called the Sudakov form factor, sums virtual gluon emissions which are also angular ordered. This is reflected in the lower limit of the first integration below

$$\Delta_S(q'_{\perp i}, z_{i-1} q'_{\perp i-1}) = \exp \left\{ - \int_{(z_{i-1} q'_{\perp i-1})^2}^{q_{\perp i}^2} \frac{dq_{\perp}^2}{q_{\perp}^2} \int_0^{1 - Q_0/q'_{\perp i}} \frac{dz}{1 - z} \bar{\alpha}_S \right\}. \quad (9)$$

The strong coupling constant $\bar{\alpha}_S = 3\alpha_S/\pi$ depends on $q_{\perp} = (1 - z)q'_{\perp}$, and the upper limit of the z integration contains the infrared cutoff Q_0 which now regularize the soft singularity in the virtual emission. The Sudakov form factor has a simple interpretation, being the probability of having no gluon radiation within the angular region $\theta_{i-1} < \theta < \theta_i$.

The function P_g is the gluon splitting function

$$P_g(z_i, q_{\perp i}^2, k_{\perp i}^2) = \frac{\bar{\alpha}_S(q_{\perp i}^2)}{1 - z_i} + \frac{\bar{\alpha}_S(k_{\perp i}^2)}{z_i} \Delta_{NS}(z_i, q_{\perp i}^2, k_{\perp i}^2), \quad (10)$$

where $k_{\perp i} = |q_{\perp 1} + \dots + q_{\perp i}|$ is the total transverse momentum of emitted gluons. The function Δ_{NS} , called the non-Sudakov form factor, sums virtual corrections relevant only in the small- z limit, with infrared singularities due to soft ($z_i = 0$) exchanged gluons

$$\begin{aligned} \Delta_{NS}(z_i, q_{\perp i}^2, k_{\perp i}^2) &= \exp \left\{ -\bar{\alpha}_S(k_{\perp i}^2) \int_{z_i}^1 \frac{dz}{z} \int \frac{dk^2}{k^2} \theta(k_{\perp i} - k) \theta(k - zq_{\perp i}) \right\} \\ &= \exp \left\{ -\bar{\alpha}_S(k_{\perp i}^2) \ln\left(\frac{1}{z_i}\right) \ln\left(\frac{k_{\perp i}^2}{z_i q_{\perp i}^2}\right) \right\}, \end{aligned} \quad (11)$$

where $k_{\perp i} > q_{\perp i}$ is assumed to get the last equality. The non-Sudakov form factor screens the $1/z$ singularity in (10), suppressing radiation both for small z and $q_{\perp i} \ll k_{\perp i}/\sqrt{z_i}$.

In the **one-loop** approximation the phase space ordering condition (7) implies that $z_{i-1} = 1$ both in the first step function in (8) and in the Sudakov form factor (9). In addition, the non-Sudakov form factor $\Delta_{NS} = 1$ since the small- z virtual corrections are relevant only in the all-loop approximation.

2.3 Gluon structure function

The unintegrated gluon structure function $\mathcal{F}(x, \mathbf{k}_{\perp}, \mu)$, which obeys the CCFM equation [2, 3], describes the probability of finding a gluon with a longitudinal momentum fraction x and transverse momentum \mathbf{k}_{\perp} at the hard scale μ , being related to the maximal angle of the emitted gluon. The additional dependence of \mathcal{F} on the hard scale is a particular feature of the CCFM equation, in contrast to the BFKL equation that, being conformally invariant, does not introduce an additional scale into the unintegrated gluon structure function.

The CCFM equation allows one to represent \mathcal{F} as a branching process with the help of the branching probabilities (8)

$$\mathcal{F}(x, \mathbf{k}_{\perp}, \mu, q_0) = \delta(x - x_0) \delta^2(\mathbf{k}_{\perp} - \mathbf{k}_{\perp 0}) \Delta_S(\mu, q_0) \Theta(\mu - q_0) + \quad (12)$$

$$\sum_{n=1}^{\infty} \int \dots \int \Theta(\mu - z_n q'_{\perp n}) \Delta_S(\mu, z_n q'_{\perp n}) \left\{ \prod_{i=1}^n d\Pi_i \right\} \delta(x - x_n) \delta^2(\mathbf{k}_{\perp} - \mathbf{k}_{\perp n}),$$

where $(x_n, \mathbf{k}_{\perp n})$ are parameters of the last exchanged gluon momentum in the chain: $k_n = x_n p + \mathbf{k}_{\perp n}$, see Fig. 1, and we explicitly indicate the presence of the collinear cutoff q_0 for the first real emission.

The integration in eq. (12) is performed over angular ordered phase space of the real gluon emission – the integration variables and their range are implicit in the branching probabilities $d\Pi_i$ (8). The additional Θ functions introduce a hard scale μ giving the upper limit for the phase space integration to be discussed in detail in section 3. The soft singularities regularized by the cutoff Q_0 in $d\Pi_i$ cancel after the phase space integration and the limit $Q_0 \rightarrow 0$ can be taken for \mathcal{F} . The collinear divergence related to the first gluon emission and regularized by q_0 stays as an important parameter in the branching procedure, providing the scale for the non-perturbative distribution $\mathcal{F}^0(x_0, \mathbf{k}_{\perp 0}, q_0)$, to be convoluted with \mathcal{F} .

The structure function \mathcal{F} integrated over transverse momentum up to the scale $\mu = Q$ becomes the usual gluon structure function (gluon density)

$$F(x, Q, q_0) \equiv \int d^2\mathbf{k}_\perp \mathcal{F}(x, \mathbf{k}_\perp, Q, q_0) \Theta(Q - |\mathbf{k}_\perp|) . \quad (13)$$

We are interested in the Q^2 dependence (evolution) of F at small x given by the CCFM equation, where for simplicity the fixed strong coupling constant $\bar{\alpha}_S$ is assumed. The result, given in terms of the moments F_ω of the gluon structure function F , is the following

$$F_\omega(Q, q_0) \equiv \int_0^1 dx x^\omega F(x, Q, q_0) = \left(\frac{Q^2}{q_0^2}\right)^{\gamma(\bar{\alpha}_S/\omega)} , \quad (14)$$

where the gluon anomalous dimension γ is equal to that obtained in the analysis of the BFKL equation

$$\gamma\left(\frac{\bar{\alpha}_S}{\omega}\right) = \gamma^{BFKL}\left(\frac{\bar{\alpha}_S}{\omega}\right) = \frac{\bar{\alpha}_S}{\omega} + 2\zeta_3\left(\frac{\bar{\alpha}_S}{\omega}\right)^4 + 2\zeta_5\left(\frac{\bar{\alpha}_S}{\omega}\right)^6 + \dots , \quad (15)$$

and ζ_i is the Riemann zeta function.

It should be noted that the BFKL anomalous dimension was derived in the all-loop (CCFM) approximation as a result of the complete cancellation of large $\log(1/x)$ powers coming from the integration over the angular ordered phase space of the real and virtual emissions. These logarithms give subleading corrections to the BFKL equation and are fully cancelled in the gluon structure function at small x . They are not cancelled, however, for more exclusive quantities, and in such cases the all-loop approximation with angular ordering is essential for the proper description of exclusive processes, see [3] for recent discussion. The subleading corrections in the CCFM equation also decrease the BFKL value of the QCD Pomeron intercept $\omega_0 = (4 \ln 2)\bar{\alpha}_S$ in the asymptotic formula: $\mathcal{F}(x) \sim x^{-(1+\omega_0)}$, and reduce diffusion in the transverse momentum space, see [11, 12].

In summary, the CCFM equation is a generalization of the BFKL equation by taking into account a part of subleading $\log(1/x)$ corrections generated by angular ordering. These corrections cancel in the fully inclusive quantity like the gluon structure function (13) but give an important contribution to more exclusive quantities (e.g. gluon multiplicity).

In the one-loop approximation the small- x behaviour is given by the gluon anomalous dimension equal to the first term in expansion (15): $\gamma(\bar{\alpha}_S/\omega) = \bar{\alpha}_S/\omega$. This result is in a perfect agreement with the gluon anomalous dimension obtained from the DGLAP equation in the small- x limit.

3 Monte Carlo simulation

The cross section (1) and branching formulae (12) form the basis for the Monte Carlo generation in SMALLX.

The procedure starts with generation of an initial state parton shower, see Fig.1. In the first step the gluon momentum $k_0 = x_0 P + k_{\perp 0}$ is generated according to a given input

$\mathcal{F}(x_0, \mathbf{k}_{\perp 0})$. Then next gluon emissions are generated with distributions (8). At the i^{th} vertex, $q'_{\perp i}$ is selected with the help of the Sudakov form factor (9), and an azimuthal angle is chosen randomly to form a vector $\mathbf{q}'_{\perp i}$. The branching fraction z_i is chosen next according to distribution (10). Notice that P_g depends on the variable $k_{\perp i} = |\mathbf{k}_{\perp i-1} + \mathbf{q}_{\perp i}|$ thus, in order to simplify the generation, the approximation $\mathbf{q}_{\perp i} \simeq \mathbf{q}'_{\perp i}$ is made when the selection of z_i is done. Then the emitted gluon momentum $\mathbf{q}_{\perp i} = (1 - z_i)\mathbf{q}'_{\perp i}$ is computed and the true value of $\mathbf{k}_{\perp i}$ calculated.

The branching continues until the stopping condition is reached, i.e. for certain n we have

$$z_n q'_{\perp n} = x_n \sqrt{s} \tan(\theta_n/2) < \mu , \quad (16)$$

and $q'_{\perp n+1}$ momentum in the next emission exceeds the bound. In this case the n -gluon final state is generated. In the **all-loop** approximation the bound μ results from condition (6)

$$\theta_1 < \dots < \theta_n < \Theta , \quad (17)$$

where Θ is the emission angle of the quark-antiquark total momentum $p_Q + p_{\bar{Q}} = Yp + \bar{Y}\bar{p} + Q_{\perp}$. Thus, it is easy to see that the choice

$$\mu = x_n \sqrt{s} \tan(\Theta/2) \quad (18)$$

gives the angular ordering condition (17). In the **one-loop** approximation the stopping condition takes the form

$$q'_{\perp n} < \mu = \sqrt{Q^2 + M^2} , \quad (19)$$

where μ is given by the scale at which the hard cross section $\hat{\sigma}$ starts to be strongly suppressed as a function of the gluon virtuality k_{\perp}^2 . We will show in the forthcoming analysis that condition (19) is much more restrictive than (16) and leads to smaller values of transverse momenta than in the all-loop case.

The quark-antiquark pair can be produced provided

$$\hat{s} \equiv (k + q)^2 > 4M^2 , \quad (20)$$

where $k = k_n$ is momentum of the last gluon in the chain and $q \simeq yl + q_{\perp}$ is the photon momentum, see Fig. 1, generated with the distribution $dy/y dq_{\perp}^2/q_{\perp}^2$. If condition (20) is satisfied the hard cross section $\hat{\sigma}$ in eq. (1) is calculated and the event is accepted with a non-zero weight, otherwise the event weight is equal to zero.

In general, the non-zero weight is a product of subweights coming from the virtual photon state generation, the gluon branching and the hard scattering. At each stage of generation the subweights could become zero when momenta fall outside kinematical limits. Condition (20) is quite restrictive in this respect and only a fraction of gluonic events can produce a quark-antiquark pair.

At the end of the generation the longitudinal momentum carried by gluons is computed at the scale μ

$$P(\mu) = \int_0^1 dx xF(x, \mu) , \quad (21)$$

where F is given by eq. (13). The conservation of $P(\mu)$ is slightly violated when μ runs, thus eventually all weights are renormalized by the factor $0.5/P(\mu)$ to get gluons carrying half of the proton's momentum.

4 Monte Carlo results

We shall present the results of our first experience with the SMALLX Monte Carlo program in HERA kinematics (27.6 GeV + 820 GeV for electron and proton energy, respectively). Most of the results will be presented in the HERA laboratory frame in which the z -axis is defined by the incoming proton direction². Some results are presented in the virtual photon-proton frame (CMS frame) with the z -axis also defined by the proton direction.

We confine ourselves to the study of open charm production in DIS at small x , with the charm quark mass $M = 1.5$ GeV. This is motivated by our strategy to fix the generation parameters, in both approximations separately, in order to describe the measured at HERA inclusive quantities like structure functions. Then we compare more exclusive final state characteristics to understand the difference between the two gluon branching schemes. Within such an approach open charm production is the best process to consider since it is not spoiled by the details of the light flavours generation.

We fix the generation parameters to describe the charm contribution $F_2^{c\bar{c}}$ to the proton structure function F_2 measured in DIS processes at HERA [13]. This includes the parameters of the initial gluon distribution \mathcal{F}^0 , for which the following form is postulated

$$x_0 \mathcal{F}^0(x_0, \mathbf{k}_{\perp 0}, Q_s) = A_0 x_0^{-p_0} (1 - x_0)^{p_1} \exp(-2\mathbf{k}_{\perp 0}^2 / Q_s^2), \quad (22)$$

where the parameter Q_s also plays the role of the collinear cutoff q_0 for the first real gluon emission, and the normalization constant A_0 is determined from the momentum sum rule $P(Q_s) = 0.5$ (21). We have fixed $Q_s = 1$ GeV and $p_1 = 5$ motivated by large- x behaviour of the conventional gluon distribution. For the purpose of Monte Carlo generation we keep the non-zero value of the infrared parameter Q_0 in (8) giving the minimal transverse momenta of emitted gluons: $Q_0 = 1$ GeV. The parameter p_0 is chosen to obtain a good description of $F_2^{c\bar{c}}$ at $Q^2 = 12$ GeV², whereas the result for higher values is given by the evolution embodied in both approximations. In order to achieve that, the shapes of the initial distributions have to differ significantly: for the one-loop mode the small- x values are strongly enhanced ($p_0 = 0.4$) in comparison to the all-loop initial distribution ($p_0 = 0.0$), see the corresponding lower curves in Fig 2.

In Fig. 3 we show $F_2^{c\bar{c}}$ at $Q^2 = 12, 25$ and 45 GeV² for all-loop (solid lines) and one-loop (dotted lines) approximations with the parameters defined above. The evolution does not differ significantly once the parameters have been tuned at $Q^2 = 12$ GeV², and both modes describe $F_2^{c\bar{c}}$ in the whole measured range quite well. This result indicates that there is no significant difference between the Q^2 evolution in the two approximations when the asymptotic x -behaviour of $F_2^{c\bar{c}}$ is obtained. Notice that in the one-loop approximation the asymptotic behaviour is imposed by hand, through the steep initial gluon distribution, whereas in the all-loop mode is a result of the CCFM evolution – compare the two corresponding upper curves in Fig. 2. The dashed lines in Fig. 3, obtained from the flat ($p_0 = 0.0$) input distribution, illustrate the importance of the steep form of the initial distribution in the one-loop mode for the data description.

² This frame is also used in SMALLX to define decomposition (2): $p = P$ and $\bar{p} = l$, where P and l are the colliding proton and lepton momenta, respectively.

4.1 Gluon branching properties

Having fixed the generation parameters we compare different characteristics of the gluon branching in the two approximations for two cases. In the first case, we analyze the gluonic state generated until the stopping condition (16) or (19) is satisfied, with the event weights given only by the gluon branching procedure. In the second case, we take into account only those gluonic events which satisfy condition (20) for quark pair production, and the full event weight, with the $\gamma g \rightarrow Q\bar{Q}$ subprocess contribution $\hat{\sigma}$, is computed. We analysed the small- x DIS regime, $1.6 \cdot 10^{-4} < x_B < 1.3 \cdot 10^{-2}$ for $\langle Q^2 \rangle = 12 \text{ GeV}^2$ and $0.01 < y < 0.8$, based on the statistics of 10^7 generated events.

In Fig. 4 we show the distribution of the transverse and longitudinal components of the last exchanged gluon momentum $k_n = x_n P + k_\perp$, see Fig. 1. The most striking feature of transverse momentum distribution (two upper plots) is a dramatic difference in the hard part of the spectrum ($k_\perp > 5 \text{ GeV}$), where the hard tail in the all-loop approximation is strongly enhanced (solid lines); see also analysis ([6]). This phenomenon can be traced back to the all-loop condition (17) which imposes only an angular bound on the maximal angle for emitted gluons, in contrast to the one-loop condition (19) that also bounds their transverse momenta. Since k_\perp is the total transverse momentum of emitted gluons, $k_\perp = |q_{\perp 1} + \dots + q_{\perp n}|$, this effect is also clearly visible in the presented spectra. There is no difference in the longitudinal momentum spectra between the two approximation (two lower plots) as a result of the choice of the input distributions.

The events with the charm pair produced (“*with box*” plots) have suppressed small values of x_n and large values of k_\perp in comparison to the “*no box*” plots, where all generated gluonic events are analysed. This can be easily understood if condition (20) is written for $q \approx y l + q_\perp$ and $k \approx x_n P + k_\perp$

$$\frac{x_n}{x_B} > \frac{4M^2 + (\mathbf{k}_\perp + \mathbf{q}_\perp)^2}{Q^2}. \quad (23)$$

Clearly, large values of x_n and small values of $|\mathbf{k}_\perp|$ are favoured by quark-antiquark pair production. Therefore, the gluon distribution is dynamically suppressed in the generation of the full final state for $x = x_n < 10^{-3}$, as is seen in the lower “*with box*” plot in Fig. 4; see also [6].

The analysis of the final state real gluons, done in the same spirit, is presented in Fig. 5. The two upper plots with the gluon multiplicity distribution exhibit a pronounced difference between the branching schemes. Due to angular ordering (6) there are significantly more gluons in the all-loop scheme, and their transverse momenta can be much bigger than in the one-loop case – see the plots in the second row, where the hard tail in the all-loop q_\perp -spectrum persists. Notice that most gluons are “soft” ($q_\perp \sim 1 \text{ GeV}$) and there are significantly more “soft” gluons in the all-loop approximation. The sharp edge at 1 GeV is the result of the infrared cutoff Q_0 imposed on transverse momenta. The plots in the bottom row show transverse momentum as a function of rapidity (E_\perp flow). The difference between the two approximations in these plots reflects the fact that there are more gluons (both “soft” and “hard”) in the CCFM branching.

It is interesting to analyse the role of the hard scale (18) in the all-loop approximation, related to the maximal angle for the gluon emission. In Fig. 6 we show the same characteristics as in Fig. 5, but now the one-loop stopping condition (19) is used in the all-loop

generation. The q_{\perp} -spectrum reveals that the scale (18) is responsible for the hard tail in the all-loop approximation – the hard tail disappears when the one-loop bound (19) is imposed in the all-loop mode, while the “soft” part of the spectrum stays intact. The other all-loop characteristics are not so dramatically affected. The average number of gluons is smaller and there are less radiation events with more than $n = 4$ gluons in the “*with box*” case (upper plots). The significant difference between the generation modes persists in the E_{\perp} flow (bottom plots) since the “soft” part of the q_{\perp} -spectrum is not affected by the one-loop stopping condition. The lack of the “hard” gluons ($q_{\perp} > 5\text{GeV}$) influences mostly the E_{\perp} flow in the central rapidity region $-1 < \eta < 1$. In summary, angular ordering (17) in the all-loop approximation leads to significantly more gluons radiated into the final state with the k_{\perp} -spectrum much harder than in the one-loop approximation.

4.2 Final state analysis

In this section we study the full final state properties, including the charm-anticharm quark pair. Therefore, for each analysed event condition (20) is satisfied and the final weight is computed. Before presenting the results let us stress that we study the very nature of the CCFM and DGLAP branching schemes, since the additional effects like the final state radiation from quarks and gluons or hadronization effects are neglected. These effects remain to be included in SMALLX to make the comparison with the real exclusive data.

In Fig. 7 we show two final state characteristics discussed in the context of the BFKL signatures in the HERA data: the transverse momentum spectra [14, 15] and the transverse energy flow [16], for the small- x kinematics specified in the previous section. The presented plots reveal how important the charm and anticharm quarks are for the final state characteristics. The difference between the approximations in the hard part of the gluonic q_{\perp} -spectrum is significantly reduced by the quark q_{\perp} -distribution. However, the difference between the approximations persists, favouring harder spectrum in the all-loop mode which stays in a qualitative agreement with the recent HERA data [15]. The E_{\perp} flow is less affected by the quark inclusion, especially in the forward region, but we expect significant hadronization corrections in this region.

In Fig. 8 we show the mean transverse energy flow $\langle E_T \rangle$ in the central region of pseudorapidity in the γp CMS frame for several values of x . $\langle E_T \rangle$ decreases with increasing x for the all-loop generation mode, and increases in the one-loop case. This result is in a qualitative agreement with the semi-analytical calculations done in [16], which are based on the BFKL and DGLAP equations.

The diffusion of the gluon transverse momenta k_{\perp} along the gluon chain as x_n decreases can result in large values of k_{\perp} in the all-loop approximation, see Fig. 4. This phenomenon leads to azimuthal decorrelation between the quark and antiquark momenta [17]. In Fig. 9 we show the distribution of the difference $\Delta\phi$ between the azimuthal angles of the quark and antiquark momenta, calculated in the γp CMS frame, for two different values of the Bjorken variable x_B . In the all-loop mode the distribution shows weakening of the azimuthal (back-to-back) correlation as x decreases, while for the one-loop case this effect is not observed, and the distribution is concentrated around $\Delta\phi = \pi$, independent of x values.

In Fig. 10 we present another widely advertised signature of the BFKL dynamics at HERA: the cross section for forward jet production [18], where the jets were chosen as in the H1 analysis [19]. In this process a forward jet with respect to the proton direction with transverse momentum $q_{\perp} \sim Q$ is measured, where Q is the virtuality of the photon. The cross section for such a measurement is significantly enhanced as a result of gluonic emissions populating the rapidity region between the forward jet and the virtual photon. The original proposition [18] concerns the gluonic emission in the Regge kinematics, but in view of discussion in [3] the angular ordered kinematics imposed in the CCFM scheme is more appropriate. We remind the reader that all our results refer to charm production, so that the presented forward jet cross sections are much smaller than those presented in [19].

The total forward jet cross sections, shown in the upper plot of Fig. 10 as a function of x_B for the two generation modes, differ significantly. The all-loop cross section is bigger and much steeper than in the one-loop approximation. The two lower plots with the pure gluonic and pure quark forward jet cross sections explain the reason for the difference seen in the upper plot. In the all-loop approximation the total cross section is dominated by the gluonic forward jet contribution and the pure quark component is almost negligible for the smallest x_B values, whereas in the one-loop mode the gluon and quark contributions are comparable, and much smaller than the gluonic cross section in the all-loop case. Clearly, forward jet production is a good process to discriminate between the two gluon branching schemes.

5 Conclusions and outlook

We have presented Monte Carlo studies of angular ordering effects in initial state gluon radiation in the small- x HERA kinematics, described by the CCFM (all-loop) branching scheme. The studies have shown the relevance of the CCFM approximation in the description of exclusive processes in DIS at HERA. In contrast to the conventional DGLAP (one-loop) approximation the CCFM scheme allows more gluons in the final state with a much broader transverse momentum spectrum. As we have shown this is the result of the angular ordering condition (17) imposed on the phase space of gluon emissions in the all-loop approximation.

The gluonic spectra are altered by the quark pair production but the angular ordering effects are still visible in the presented characteristics. The most spectacular results are the azimuthal angle decorrelation for the heavy quarks – a direct consequence of k_{\perp} -diffusion along the gluon chain in the CCFM scheme, and forward jet production. The rest of the results may strongly depend on such effects like the final state branching, hadronization or inclusion of quarks in initial state radiation. Therefore the additional effort is necessary to include these effects into SMALLX, before the meaningful comparison with HERA data could be done. We hope to report on progress in this direction in the near future.

Acknowledgements

We are grateful to Bryan Webber for providing us with his Monte Carlo program SMALLX and for valuable discussions. Discussions with Gunnar Ingelman, Hannes Jung, Michael Kuhlen, Jan Kwieciński, Sabina Lang, Claire Lewis, Ewelina Łobodzińska, Giuseppe Marchesini, Alan Martin and Peter Sutton are gratefully acknowledged. We also thank John Campbell for a careful reading of the manuscript. K.G thanks the Royal Society for financial support and the Department of Physics of the University of Durham for its warm hospitality. This research has been supported in part by the Polish State Committee for Scientific Research, grants no.2 P03B 231 08, 2 P03B 089 13 and 2 P03B 055 13.

References

- [1] M.Ciafaloni, Nucl.Phys. **B296** (1988) 49.
- [2] S.Catani, F.Fiorani, G.Marchesini, Phys. Lett. **B234** (1990) 339, Nucl.Phys. **B336** (1990) 18;
S.Catani, F.Fiorani, G.Marchesini, G.Oriani, Nucl. Phys. **B361** (1991) 645.
- [3] G.Marchesini, Nucl. Phys. **B445** (1995) 49.
- [4] L.N.Lipatov, Sov.J.Nucl.Phys. **23** (1976) 642;
V.S.Fadin, E.A.Kuraev, L.N.Lipatov, Phys. Lett. **B60** (1975) 50;
E.A.Kuraev, L.N.Lipatov, V.S.Fadin, Sov. Phys. JETP **44** (1976) 45, Sov. Phys. JETP **45** (1977) 199;
Ya.Ya.Balitsky, L.N.Lipatov, Sov. J. Nucl.Phys. **28** (1978) 822.
- [5] G.Marchesini, B.Webber, Nucl. Phys. **B349** (1991) 617.
- [6] G.Marchesini, B.Webber, Nucl. Phys. **B386** (1992) 215.
- [7] B.Anderson, G.Gustafson and J.Samuelsson, Nucl. Phys. **B463** (1996) 217;
B.Anderson, G.Gustafson, H.Kharraziha and J.Samuelsson, Z.Phys. **C71** (1996) 613;
G.Gustafson, H.Kharraziha and L. Lönnblad, NORDITA-96-67-P, Oct. 1996 and in Proceedings of the Workshop "Future physics at HERA", Hamburg 1995/96, 620;
H.Kharraziha and L. Lönnblad, LU-TP 97-21, NORDITA-97/54 P, hep-ph/9709424.
- [8] V.N.Gribov, L.N.Lipatov, Sov.J.Nucl.Phys. **15** (1992) 438, 675;
G.Altarelli, G.Parisi, Nucl.Phys.**B126** (1977) 297;
Yu.L.Dokshitzer, Sov.Phys.JETP **46** (1977) 641.
- [9] A.Basseto, M.Ciafaloni, G.Marchesini, Phys. Rep. **100** (1983) 201;
Yu.I.Dokshitzer, V.A.Khoze, S.L.Troyan, A.H.Mueller, Rev. Mod. Phys. **60** (1988) 373.
- [10] S.Catani, M.Ciafaloni, F.Hautmann, Phys. Lett **242** (1990) 97, Nucl. Phys. **366** (1991) 135;
J.C.Collins, R.K.Ellis, **360** (1991) 3.;
E.M.Levin, M.G.Ryskin, Yu.M.Shabelskii, A.G.Shuvaev, Sov. J. Nucl. Phys. **54** (1991) 867.
- [11] J.Kwieciński, A.Martin and P.Sutton, Phys. Rev. **D52** (1995) 1445, Phys. Rev. **D53** (1996) 6094, Z.Phys. **C71** (1996) 585.
- [12] G.Botazzi, G.Marchesini, G.P.Salam and M.Scorletti, hep-ph/9702418, hep-ph/9705233, hep-ph/9707237, hep-ph/9707383.
- [13] H1 Collaboration, C.Adloff *et al.*, Z.Phys. **C72** (1996) 593.
- [14] M.Kuhlen, Phys. Lett. **382** (1996) 441;
J.Kwieciński, S.Lang and A.D.Martin, DTP/97/56, hep-ph/9707240.

- [15] H1 Collaboration, C.Adloff *et al.*, Nucl. Phys. **B485** (1997) 3.
- [16] H1 Collaboration, I.Abt *et al.* Z.Phys. **C63** (1994) 377;
J.Kwieciński, A.D.Martin, P.J.Sutton and K.Golec-Biernat, Phys.Rev. **D50** (1994) 217;
K.Golec-Biernat, J.Kwieciński, A.D.Martin and J.P.Sutton, Phys.Lett. **B335** (1994) 220.
- [17] A.J.Askew, D.Graudenz, J.Kwieciński and A.D.Martin, Phys.Lett. **B338** (1994) 92.
- [18] A.H.Mueller, Nucl. Phys.D (Proc. Suppl.) **18C** (1990) 125; J. Nucl. Phys. **G17** (1991) 1443;
W.K.Tang, Phys. Lett. **B278** (1992) 363;
J.Kwieciński, A.D.Martin and P.J.Sutton, Phys. Lett **B287** (1992) 254, Nucl. Phys. B (Proc. Suppl.) **29A** (1992) 67;
J.Bartels, V.Del Duca, A.De Roeck, D.Graudenz and M.Wüsthoff, Phys. Lett. **B384** (1996) 300.
- [19] H1 Collaboration, C.Adloff *et al.*, contributed paper pa03-049, ICHEP '96, Warsaw, Poland, July 1996.

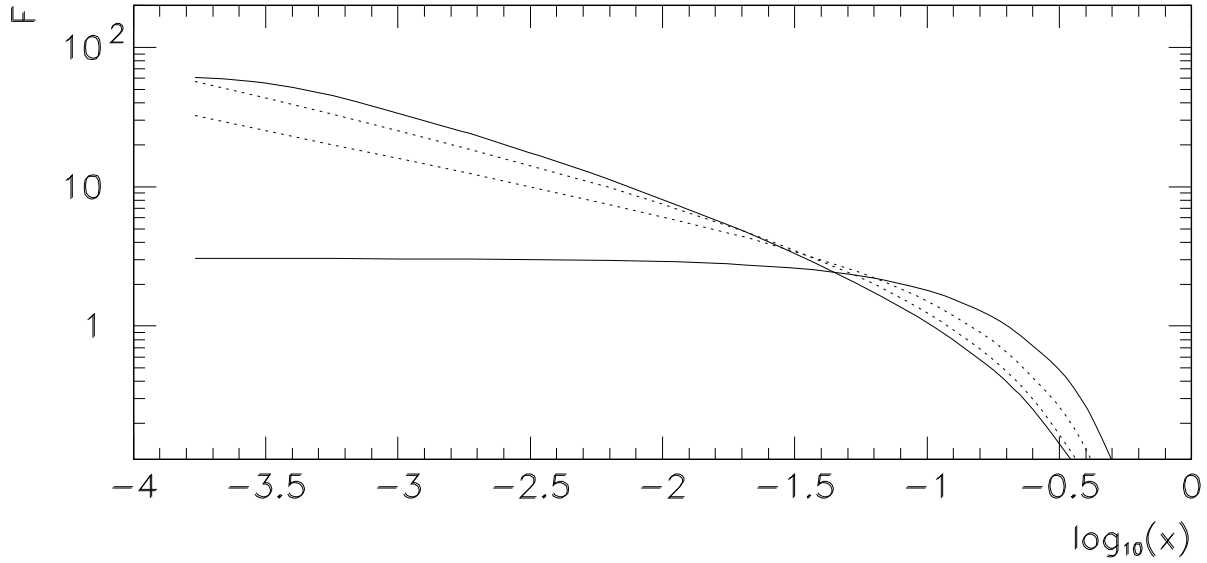


Figure 2: The integrated gluon distribution F in all-loop (solid) and one-loop (dotted) schemes at the initial scale 1 GeV^2 (the corresponding lower curves), and after evolution to $\langle Q^2 \rangle = 12 \text{ GeV}^2$ (the corresponding upper curves).

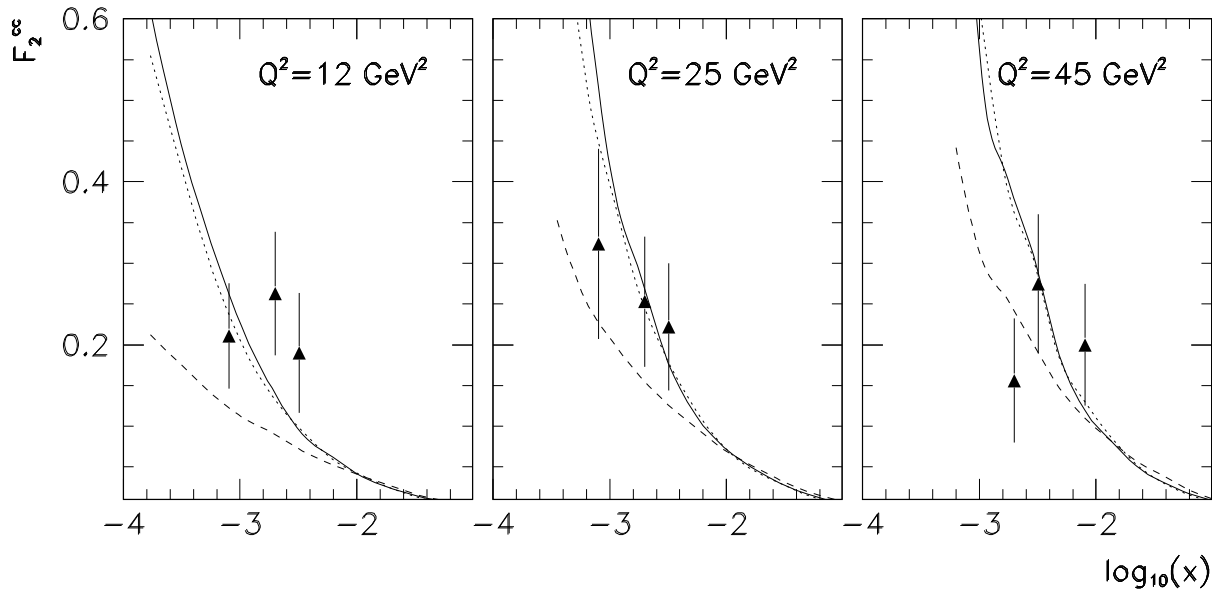


Figure 3: F_2^{sc} in the all-loop (solid lines) and one-loop (dotted lines) approximations. The dashed lines are obtained for the flat input distribution in the one-loop mode.

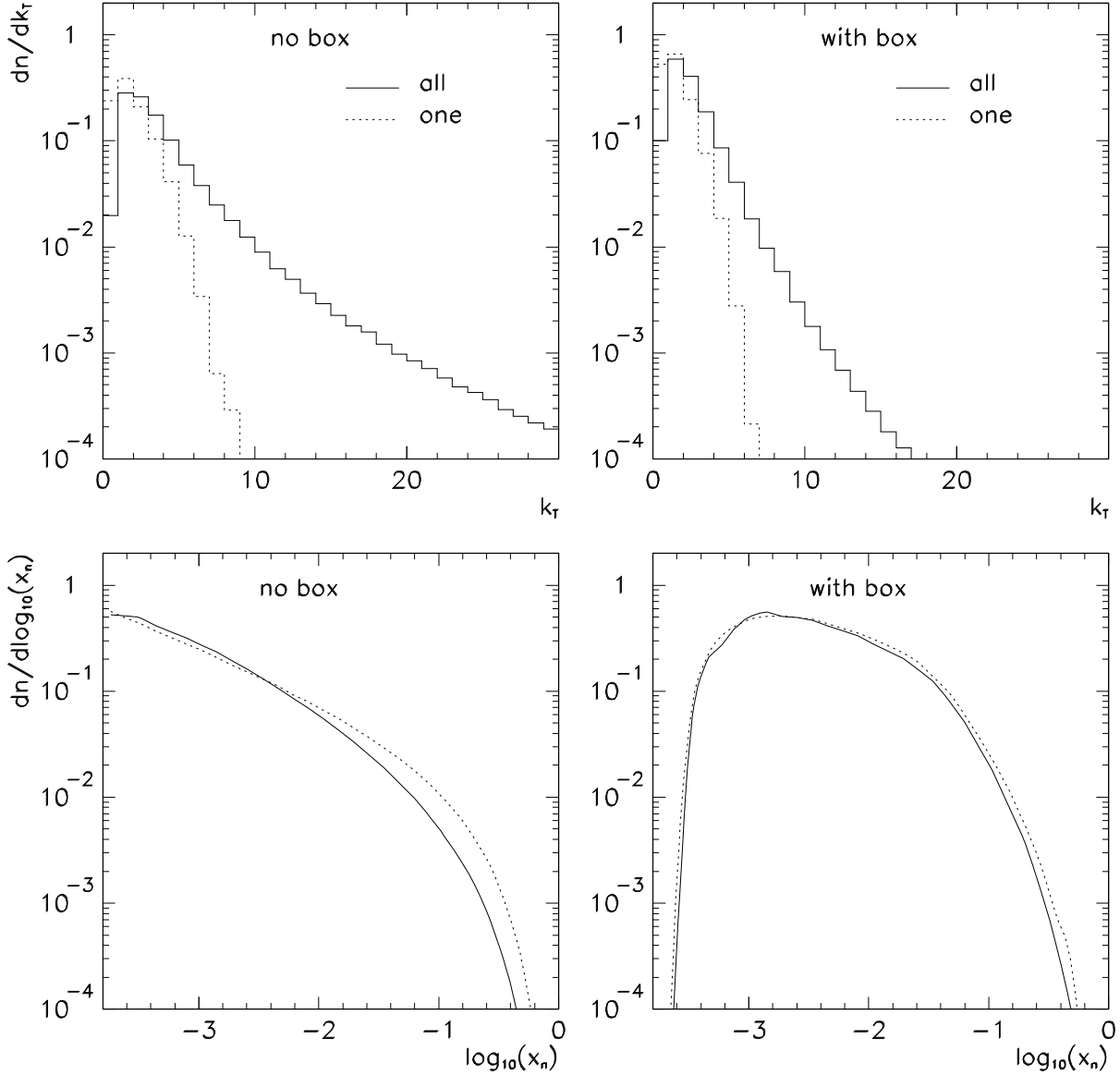


Figure 4: The transverse k_{\perp} and longitudinal x_n momentum distributions of the last exchanged gluon for all gluonic events (“no box”) and the events with the quark pair produced (“with box”) in the all-loop (solid) and one-loop (dotted) approximations.

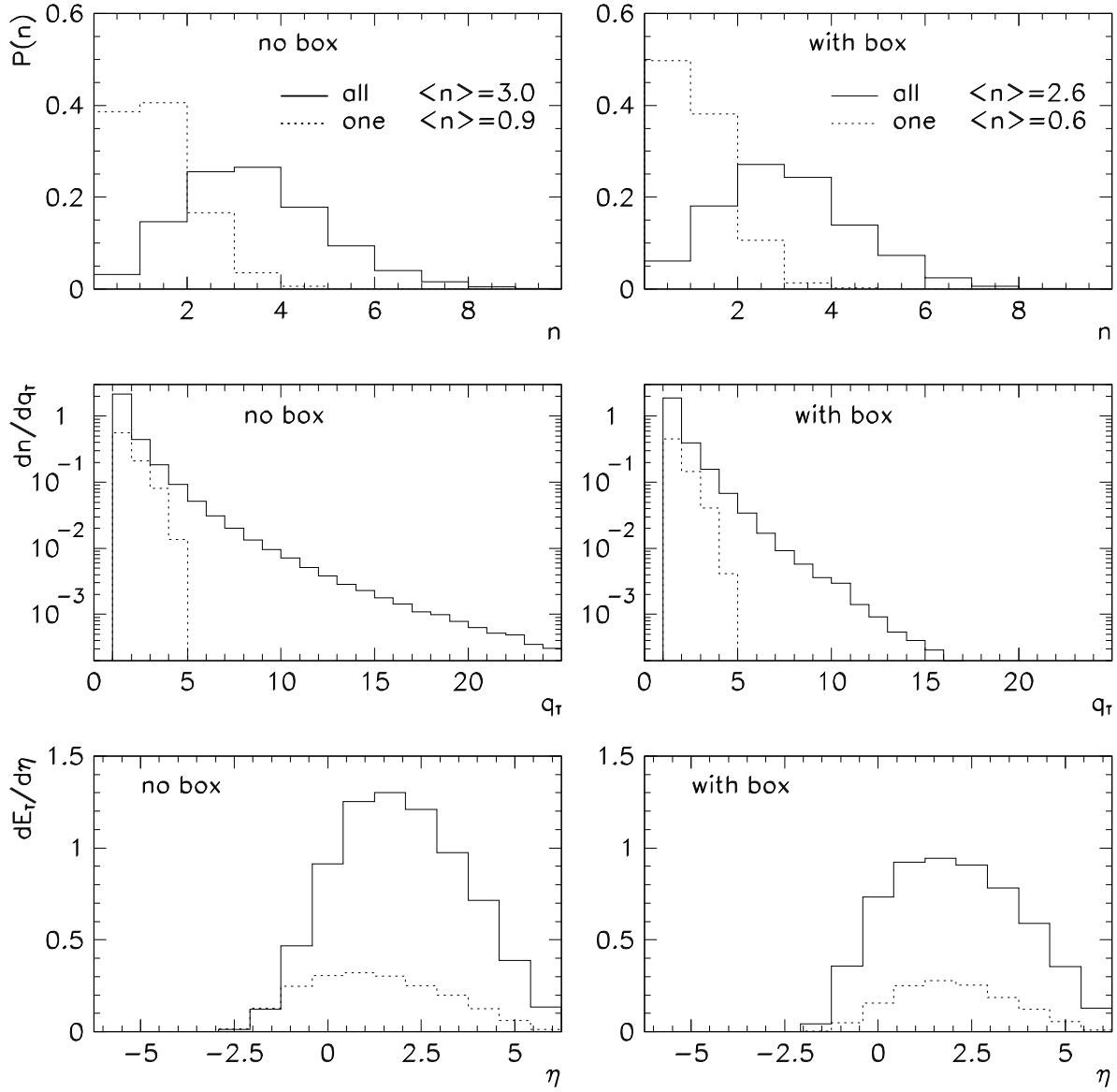


Figure 5: The final state gluon characteristics in the all-loop (solid) and one-loop (dotted) approximations. The influence of the quark pair production is shown on the right (“with box” plots).

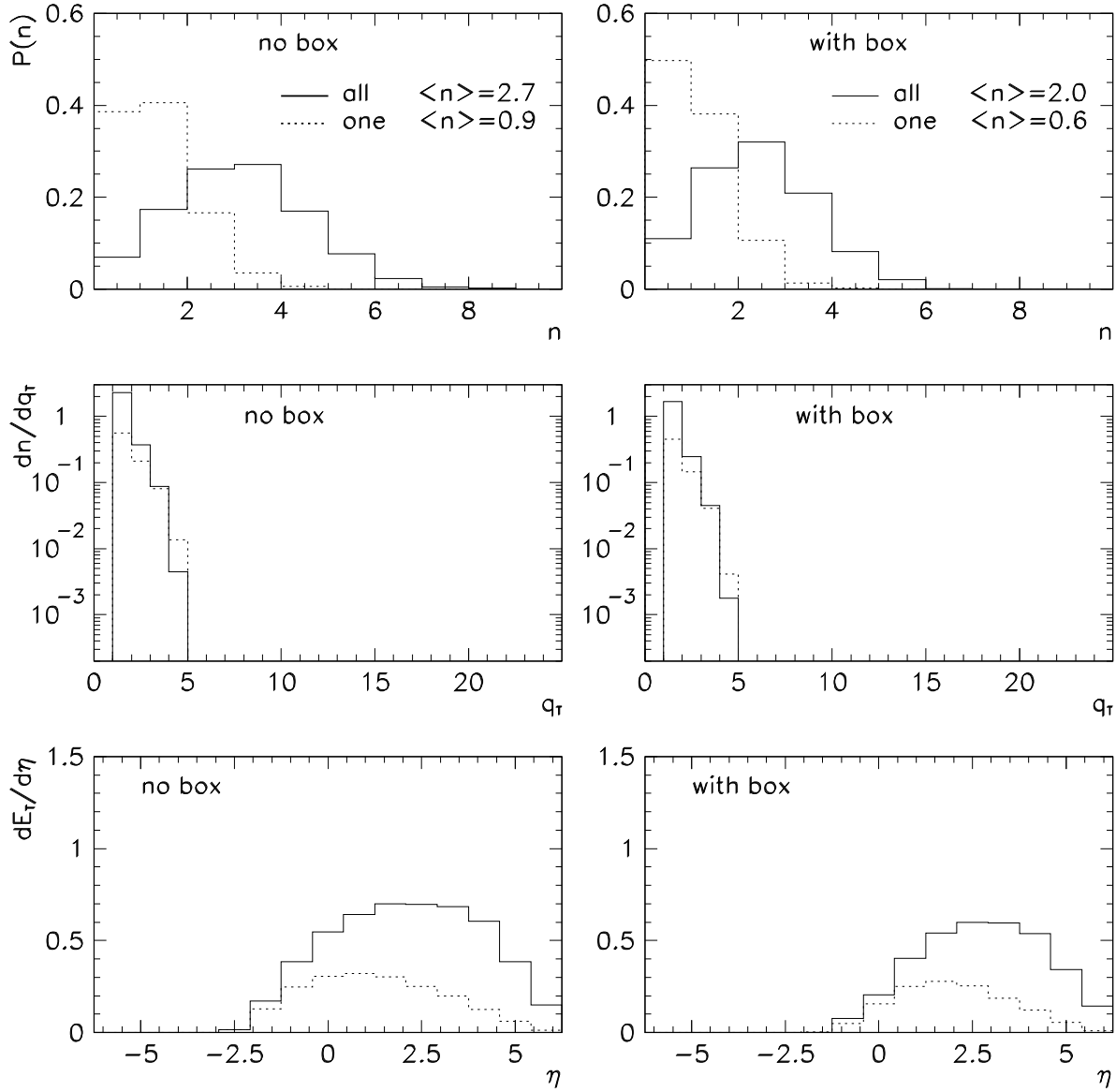


Figure 6: The same as Fig. 5 but now the one-loop stopping condition is imposed in the all-loop generation.

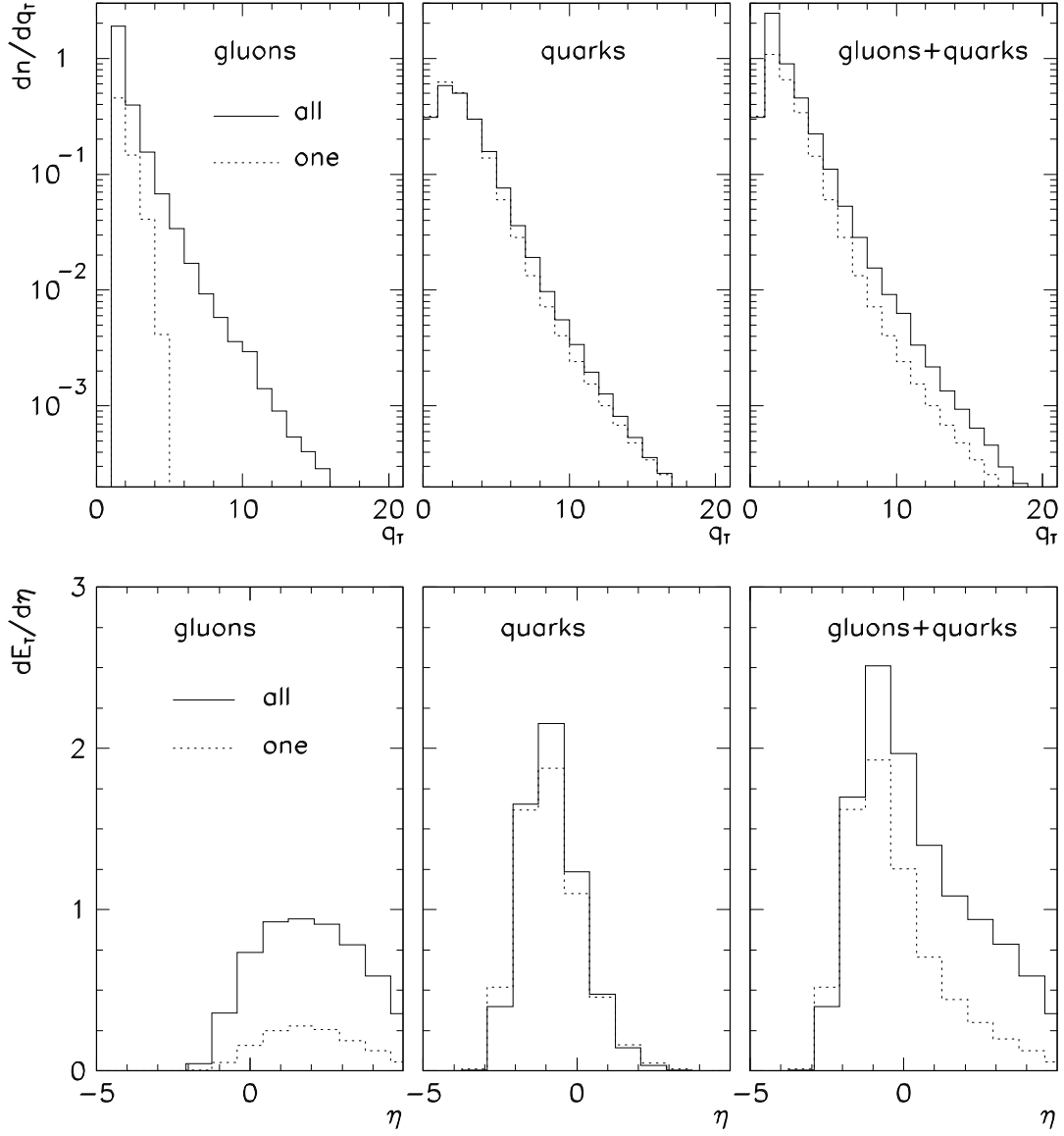


Figure 7: The k_{\perp} -spectrum and E_T flow for final state partons. Gluon and quark contributions are shown separately.

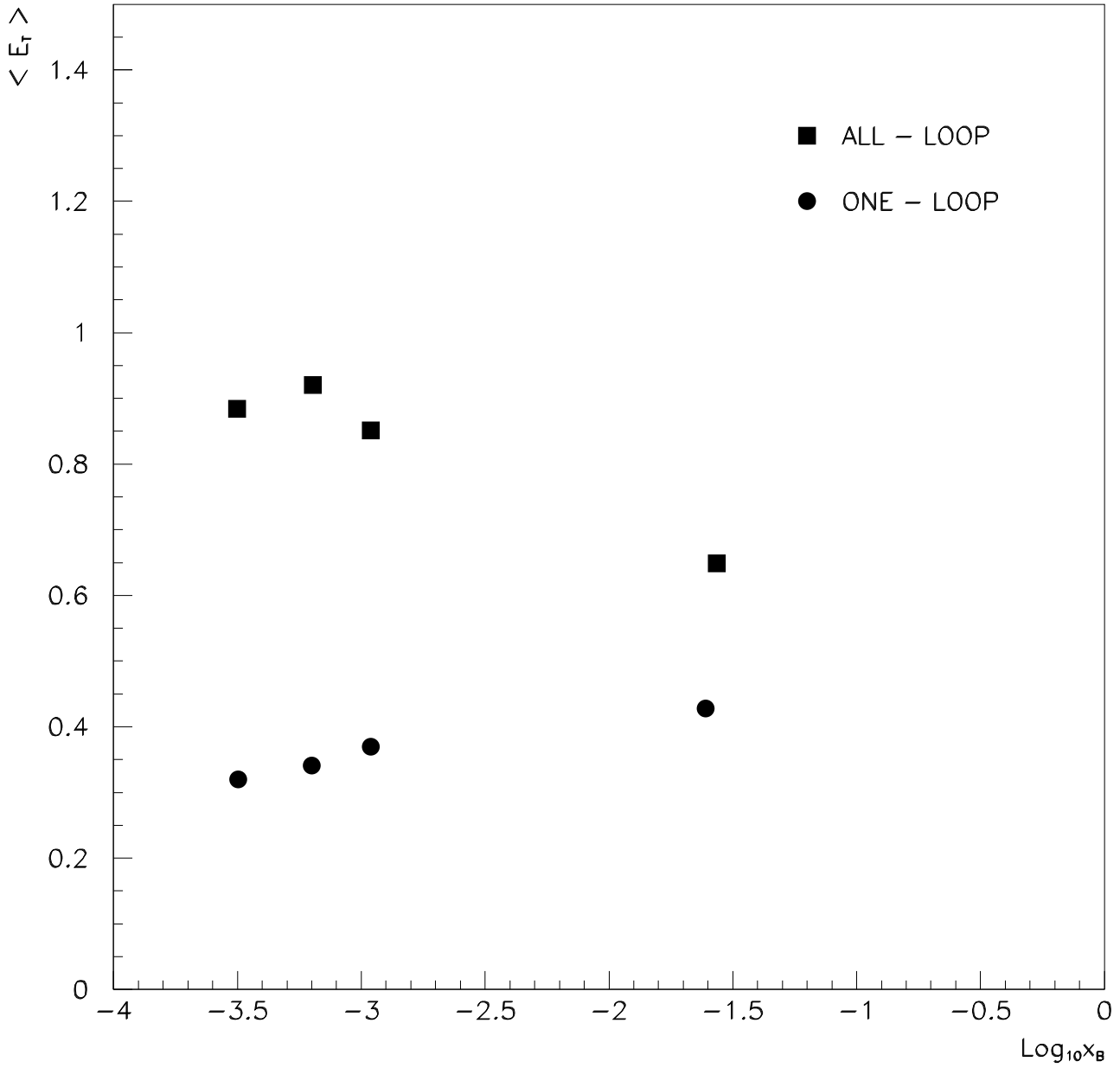


Figure 8: The average value of the transverse energy in the central rapidity region $-0.5 < \eta^* < 0.5$ in the γp CMS frame as a function of the Bjorken variable x .

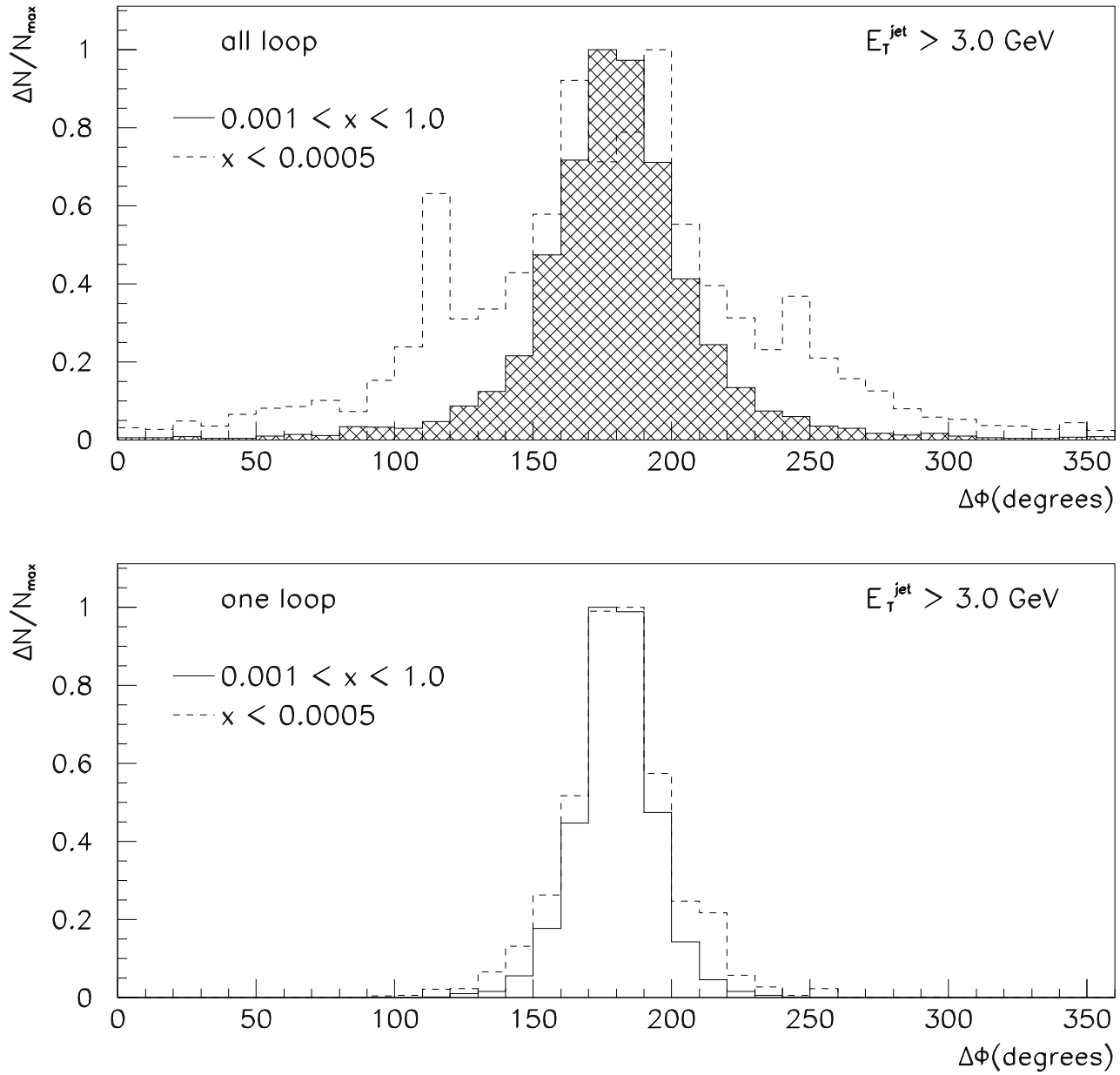


Figure 9: The difference between the azimuthal angles of the quark and antiquark momenta in the γp CMS frame for different values of the Bjorken variable x .

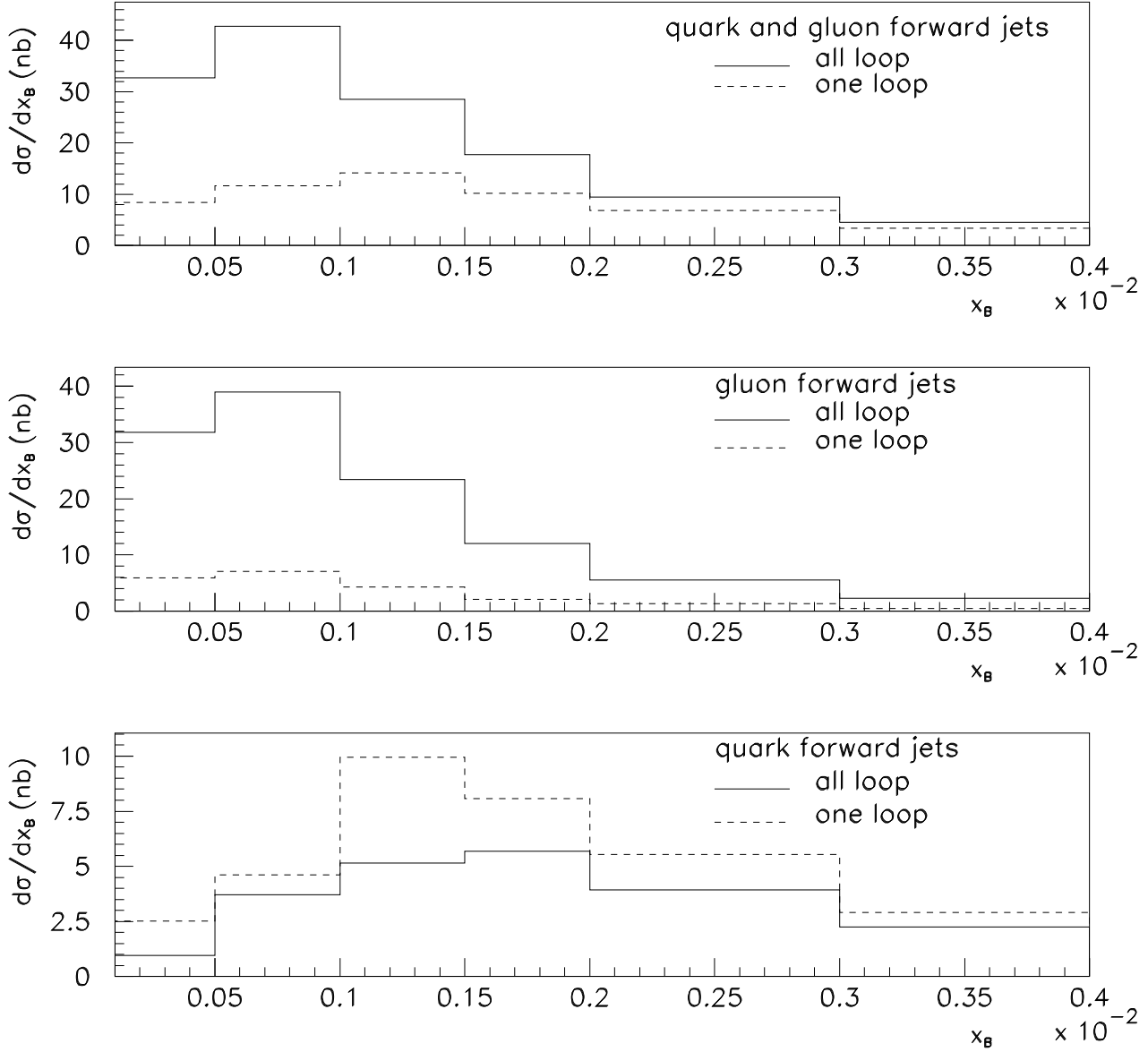


Figure 10: The forward jet cross section as a function of the Bjorken variable x_B , with the H1 analysis cuts. The gluon and quark forward jet cross sections are shown on separate plots.